

Electromagnetic Self-Organization and Transport Barrier Relaxations in Fusion Plasmas

G. Fuhr^{1,2}, S. Benkadda^{1,2}, P. Beyer^{1,2}, M. Leconte^{1,2}, X. Garbet³, I. Sandberg⁴, H. Isliker⁵, D. Reiser⁶, I. Caldas⁷, Z.O. Guimarães-Filho⁷, S. Hamaguchi^{8,1}

¹France-Japan Magnetic Fusion Laboratory, LIA 336 CNRS ²Equipe Dynamique des Systèmes Complexes, UMR 6633 CNRS-Université de Provence, Marseille ³IRFM, Association EURATOM, CEA, CEA Cadarache, France ⁴National Technical University of Athens, Association EuratomHellenic Republic, Department of Electrical and Computer Engineering GR–157 73 Athens, Greece ⁵Department of Physics, Aristotle University of Thessaloniki, GR-541 24 Thessaloniki, Greece ⁶Institut für Energieforschung-Plasmaphysik, Forschungszentrum Jülich GmbH, EURATOM Association, Germany ⁷Universidade de São Paulo, Brazil ⁸Center for Atomic and Molecular Technologies, Osaka University, Japan

Abstract. Several aspects of plasma turbulence and transport at a tokamak edge have been studied by three dimensional numerical simulations of resistive ballooning turbulence in a toroidal geometry. These simulations have been realized with a three dimensional global code which calculates the evolution of the pressure and the electrostatic potential at the plasma edge and also includes self-consistent electromagnetic fluctuations. The level of magnetic fluctuations present in the system is linked to the plasma beta (the ratio between the kinetic pressure and the magnetic pressure). The competition between different mechanisms for driving flows (Reynolds stress, Maxwell tensor) is studied as a function of beta. In order to characterize the stationary turbulent state of the plasma we use standard and sophisticated statistical tools, e.g. probability density functions (PDFs) and the Extended Self-Similarity method. We also study the dynamics of transport barriers at the plasma edge that are key elements of high confinement modes (H–modes) in fusion devices. In these simulations the transport barrier exhibits intermittent relaxation cycles. It is found that magnetic fluctuations have negligible influence on the relaxation process while the magnetic activity is enhanced during these relaxations, in agreement with experimental observations. Additionally, the simulations reveal that resonant magnetic perturbations (RMPs) have a stabilizing effect on the transport barrier relaxations.

1. Introduction

In hot magnetized plasmas, the main component of the radial transport is supposed to be anomalous, e.g. not due to collisions and diffusion processes. This radial transport is strongly linked to the presence of instabilities in the plasma which give rise to both, electrostatic and magnetic perturbations. Experimental measurements of fluctuation levels on typical fusion devices reveal that electrostatic fluctuations are dominant and can reach a level of 50% at the plasma edge. Magnetic fluctuations are much smaller in such experiments. However, as even small magnetic perturbations ($\sim 10^{-4}$) can locally modify the topology of the magnetic surfaces, such fluctuations play an important role with respect to the transport properties of the plasma. Here, we show results from turbulence simulations at a tokamak plasma edge, realized with a three dimensional global code, evolving self-consistently electromagnetic fluctuations as well as the pressure and ExB velocity profiles. We first concentrate on the characterization of turbulent self-organization and the competition between different mechanisms for driving flows (Reynolds stress, Maxwell tensor). Then, we focus on the dynamics of transport barriers. Transport barriers at plasma edge are a key elements of high confinement modes (H–modes) in fusion devices. In general, they are not stable but relax quasi-periodically. Experimental observations have revealed a strong magnetic activity associated to such relaxation events. The turbulence simulations presented here reproduce complete cycles of transport barrier relaxations in presence of self-consistent electromagnetic fluctuations.

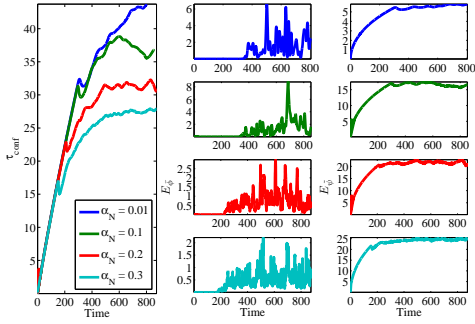


Figure 1: Evolution of confinement time (left), mean electrostatic potential (middle) and electromagnetic fluctuations (right) in time for different value of α_N .

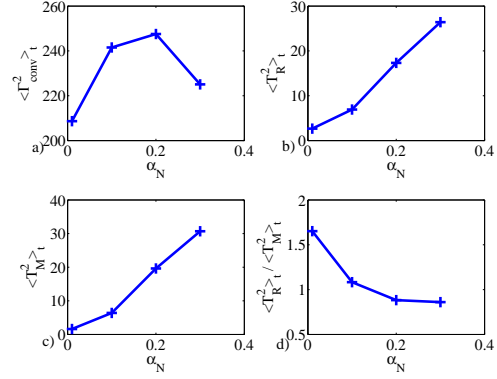


Figure 2: Averaged value, respectively to Eq. , for turbulent flux (a), Reynolds stress (b) and Maxwell tensor (c). Ratio between Reynolds stress and Maxwell tensor for different values of the α_N parameter (d).

Electromagnetic plasma edge turbulence is simulated here using a resistive ballooning model. The latter is based on fluid equations for the normalized electrostatic potential ϕ , electromagnetic flux ψ and pressure p [1].

$$\partial_t \nabla_{\perp}^2 \phi + \{\phi, \nabla_{\perp}^2 \phi\} = -\frac{1}{\alpha_N} \nabla_{\parallel} \nabla_{\perp}^2 \psi - \mathbf{G}p + \nu \nabla_{\perp}^4 \phi, \quad (1)$$

$$\partial_t p + \{\phi, p\} = \delta_c \mathbf{G}\phi + \chi_{\parallel} \nabla_{\parallel}^2 p + \chi_{\perp} \nabla_{\perp}^2 p + S, \quad (2)$$

$$\partial_t \psi = -\nabla_{\parallel} \phi + \frac{1}{\alpha_N} \nabla_{\perp}^2 \psi. \quad (3)$$

Equation (1) corresponds to the normalized charge balance, Eq. (2) is the normalized energy balance and Eq. (3) corresponds to the Ohm's Law. ∇_{\perp} and ∇_{\parallel} respectively correspond to the parallel and perpendicular gradients along field lines. \mathbf{G} is the curvature operator, ν represents the viscosity, χ_{\parallel} and χ_{\perp} are the parallel and perpendicular thermal diffusivities respectively. Time is normalized by the resistive interchange time $\tau_{\text{int}} = \sqrt{R_0 L_p / 2} / c_S$, where c_S is the sound speed, R_0 is the major radius and L_p is the pressure gradient length. The perpendicular and parallel length scales are the resistive ballooning length $\xi_{\text{bal}} = \sqrt{\rho \eta_{\parallel} / \tau_{\text{int}} L_s / B_0}$ and the magnetic shear length L_s , respectively. Here, ρ is the mass density and η_{\parallel} the parallel resistivity. $q(r)$ stands for the safety factor which measures the magnetic field line pitch. α_N is expressed by $\alpha = q^2 \alpha_N$ where α is the normalized pressure gradient typically used to express the stability limit for ideal ballooning modes, $\alpha \simeq 1$ [2]. α_N is also related to the β parameter (the ratio of kinetic pressure to the magnetic pressure) through $\alpha_N = \beta L_s^2 / (R_0 L_p)$. The parameter δ_c is defined by $\delta_c = 2\Gamma L_p / R_0$, Γ is the heat capacity ratio ($\Gamma = 5/3$). The last term of the r.h.s. of Eq. (2), $S(r)$ represents a constant energy source.

2. Self-Organization of Plasma in presence of EM fluctuations.

Fig. (1) shows the time evolution of the edge confinement time τ_{conf} , the energy associated with the mean electrostatic potential $E_{\bar{\phi}}$ as well as the energy associated with electromagnetic fluctuations $E_{\bar{\psi}}$ for different values of the α_N parameter, ranging from $\alpha_N = 0.01$ to $\alpha_N = 0.3$.

Here, the edge confinement time and the energies are defined as

$$\tau_{\text{conf}} = \frac{1}{\Gamma_{\text{tot}}} \int_V p(r, \theta, \varphi, t) dV \quad E_{\bar{\phi}}(t) = \sqrt{\int_R |\bar{\phi}(r, t)|^2 dr} \quad E_{\tilde{\psi}}(t) = \sqrt{\int_V |\tilde{\psi}(r, \theta, \varphi, t)|^2 dV} \quad (4)$$

where $\Gamma_{\text{tot}} = \int_V S(r) dV$ is the constant energy flux coming from the plasma core and V is the simulated volume at the plasma edge. A strong impact of the α_N parameter on the confinement time is observed. In a statistically stationary state, the level of τ_{conf} is lower by nearly 40% in the case of the highest value of α_N compared to the one with the lowest value of α_N . The level of magnetic fluctuations is found to increase with increasing α_N (Fig. (1), right column). However, as the parallel diffusivity is set to zero in these simulations ($\chi_{\parallel} = 0$), the magnetic perturbations do not contribute to the evolution of the pressure [i.e. $\Gamma_{\delta B} = 0$ in Eq. (6) presented below] and therefore the decrease of τ_{conf} with α_N can not be attributed directly to the increase of the magnetic fluctuations and a different mechanism has to be invoked. We therefore study the energy associated with the mean electric potential, $E_{\bar{\phi}}$, which is linked via the ExB drift to a mean poloidal rotation of the plasma. As can be seen from Fig. (1), middle column, the level of $E_{\bar{\phi}}$ in the stationary state is decreasing with α_N and therefore the mean plasma rotation is decreasing. As this rotation typically has a stabilizing effect on the turbulence via a shearing of convective cells, the decrease of $E_{\bar{\phi}}$ is expected to lead to a higher turbulence level and therefore a lower confinement time. The competing mechanism for the generation of the mean poloidal rotation can be studied by averaging poloidally and toroidally the equation for the electrostatic potential, Eq. (1). The corresponding equation of the poloidal flow is :

$$\partial_t \bar{v}_{\theta} = -\partial_r (T_R + T_M + T_V) - \langle Gp \rangle_{\theta\varphi}, \quad (5)$$

where the notation $\langle \rangle_{\theta\varphi}$ stands for the average in the poloidal and toroidal directions; $\bar{v}_{\theta} = \langle v_{\theta} \rangle_{\theta\varphi}$ is the flow profile and $\tilde{v}_{r,\theta} = v_{r,\theta} - \bar{v}_{r,\theta}$ is the fluctuating part of the radial (respectively poloidal) velocity, $\tilde{\psi}$ is the fluctuating part of the magnetic flux. The Reynolds stress $T_R = \langle \tilde{v}_{\theta} \tilde{v}_r \rangle_{\theta\varphi}$ and the Maxwell tensor $T_M = \langle \partial_{\theta} \tilde{\psi} \partial_r \tilde{\psi} \rangle_{\theta\varphi}$ are represented by the first two terms of Eq. (7), T_V , corresponds to the viscosity effects. Following the equation for the pressure profile,

$$\partial_t \bar{p} = -\partial_r (\Gamma_{\text{Conv}} + \Gamma_{\text{Coll}} + \Gamma_{\delta B}) + \delta_c \langle G\phi \rangle_{\theta\varphi} + S, \quad (6)$$

the total energy flux is decomposed into three components : the convective flux $\Gamma_{\text{conv}} = \langle \bar{p} \tilde{v}_r \rangle_{\theta\varphi}$, the collisional damping $\Gamma_{\text{coll}} = -\chi_{\perp} \partial_r \bar{p}$ and the flux due to the parallel diffusivity $\Gamma_{\delta B} = -\chi_{\parallel} \langle \partial_{\theta} \tilde{\psi} \nabla_{\parallel} p \rangle_{\theta\varphi}$.

To compare the relative importance of the stresses T_R and T_M in the transport dynamics, we

study the time average of the norm of each of these tensors, defined by $\langle F^2 \rangle_t = \sqrt{\langle \int_R |F(r, t)|^2 dr \rangle_t}$. The results are plotted in Fig. (2). Both, Maxwell tensor and Reynolds stress are found to increase with α_N . However, the ratio between $\langle T_M^2 \rangle_t$ and $\langle T_R^2 \rangle_t$ decreases with α_N such that for low values of α_N , the Reynolds stress is dominant, and for $\alpha_N \geq 0.1$, Reynolds and Maxwell stresses have similar amplitudes. As the Reynolds stress is known to drive the poloidal flow [Eq. 7], we conclude that the decrease of the poloidal flow energy with increasing α_N is linked to a competition between Reynolds and Maxwell stresses.

2.1 Self-similarity

One of the most efficient tools to study the scaling and self-similarity properties of turbulence is the structure function [3]. The structure function of order q for a field u in a fully developed turbulent state is defined as [3] $S_q(u; r) = \langle |u(x+r) - u(x)|^q \rangle$, where r represents a spatial separation and $\langle \dots \rangle$ is the ensemble average. The structure function $S_q(u; \tau)$ for the

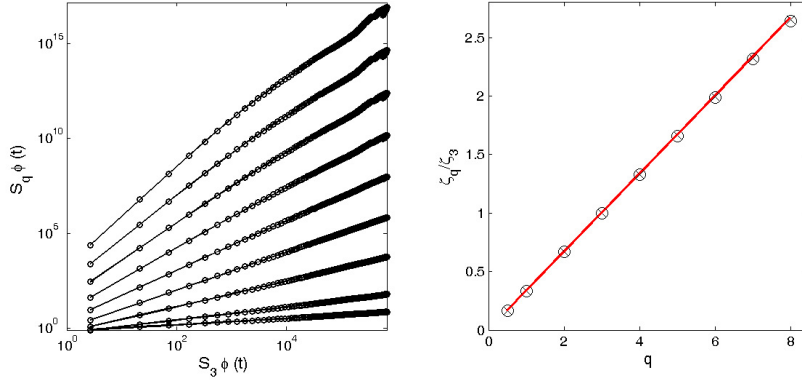


Figure 3: *The structure functions S_q ($q=0.5,1,2..8$) versus S_3 for the potential fluctuations (Left panel). The ESS relative scaling exponents of the potential ϕ (Right panel).*

temporal scales is defined similarly. We have properly calculated the temporal and the spatial structure functions for the spatio-temporal fluctuations of the potential, pressure, magnetic field and vorticity, for various values of α . When the signal u is self-similar over some range of spatial (temporal) scales, the structure function shows a power-law dependence on the scale-size, i.e. the q -th order structure function is expected to scale as $S_q \propto r^{\zeta_q}$, where ζ_q is the scaling exponent. This is theoretically the case in the inertial range of turbulence - the range of wave numbers where the dominant process is the energy transfer and not the energy injection or dissipation. However, in plasmas the different scaling regimes are not widely separated, which causes difficulties in the accurate estimate of the scaling exponents. The notion though of Extended-Self-Similarity (ESS) [4] provides a successful method that allows to extend the structure function analysis into the dissipation and the large scale region. With the ESS method, the dependence of the ratio ζ_q/ζ_3 on q can numerically be determined. For the case of RBM turbulence, we find a $q/3$ linear scaling for ζ_q/ζ_3 , which is in agreement with the structure function exponent for the potential as it is experimentally found in edge turbulence [5], indicating the mono-fractal scaling for the fluctuations.

2.2 The scaling between kurtosis and skewness

Several analyses have revealed the non-Gaussian statistics in the edge fluctuations of a number of devices. Here, we focus on the properties of the kurtosis and skewness and on the scaling between these statistical quantities. For a centered random variable \tilde{x} with variance σ^2 , skewness is defined by the $S \equiv \langle \tilde{x}^3 \rangle / \sigma^3$ and the kurtosis by $K \equiv F - 3$ where the flatness is $F \equiv \langle \tilde{x}^4 \rangle / \sigma^4$. Skewness is a measure of asymmetry of a PDF. If the left tail is heavier (more pronounced) than the right tail, the PDF has negative skewness. If the reverse is true, it has positive skewness. If the PDF is symmetric, it has zero skewness. Kurtosis (or more accurately, 'excess kurtosis') measures the excess probability (flatness) in the tails, where excess is defined in relation to a Gaussian distribution. Utilizing the results obtained by the numerical simulations of Resistive Ballooning Mode Turbulence we have calculated the values of skewness and kurtosis of the timeseries of various fluctuating fields (e.g. potential, vorticity, pressure etc.) for each grid point of the computational domain. For a significant number of time series the values of Skewness and Kurtosis show a large deviation from their Gaussian values. The K - S scatter plot is shown in Fig. (4), and it has clear a parabolic character. A least-squares fit with a quadratic polynomial yields $K = (1.476 \pm 0.006)S^2 - (0.496 \pm 0.002)$. The uncertainty in the estimated coefficients is determined as the 95% confidence limits.

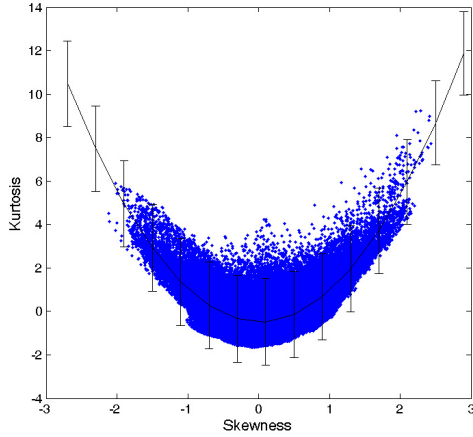


Figure 4: *Kurtosis vs. skewness computed for $\sim 3 \times 10^5$ time-series and the fitted quadratic polynomial.*

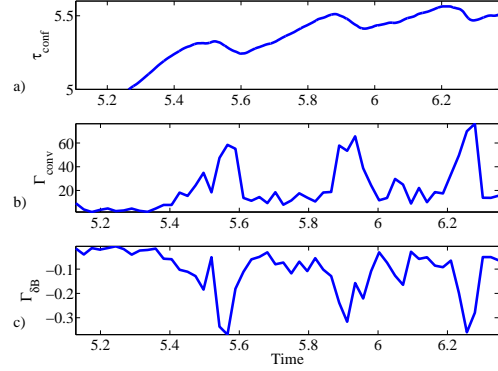


Figure 5: *Time evolution of confinement time (τ_{conf}) (a), turbulent flux (Γ_{conv}) (b) and flux due to magnetic component ($\Gamma_{\delta B}$) (c) at the center of the barrier. Here, $\omega_E = 3$, $\Gamma_{tot} = 18$, $\mu = 20$. Time is represented in units of ms based on the value of $\tau_{int} \simeq 2\mu s$. The relaxation frequency is $f_{relax} \simeq 3$ kHz.*

These results show a remarkable similarity with the experimental results presented recently in a Letter by Labit et al. [6]. The authors [6] found a unique parabolic relation, $K = (1.502 \pm 0.015)S^2 - (0.226 \pm 0.019)$, between the skewness S and kurtosis K of about ten thousand observed density fluctuation signals that are associated with drift-interchange turbulence over a broad range of experimental conditions.

Parabolic relations of this kind have been found in different physical systems. In a recent report [7], Krommes discussed the remarkable similarity in the K-S relation of Torpex density fluctuations with the K-S relation of sea-surface temperature fluctuations, and suggested a generalized non-linear Langevin theory that includes linear wave propagation for its explanation.

3. Barrier relaxation oscillations and stabilization via static magnetic perturbation.

In the present model, a transport barrier is generated by an imposed shear flow (v_{imp}). A corresponding drive is added to the equation of the poloidal flow:

$$\partial_t \bar{v}_\theta = -\partial_r \left(T_R + T_M + T_V - \langle Gp \rangle_{\theta\phi} + \mu(\bar{v}_\theta - v_{imp}) \right), \quad (7)$$

where the notation $\langle \rangle_{\theta\phi}$ stands for the average in the poloidal and toroidal directions; $\bar{v}_\theta = \langle v_\theta \rangle_{\theta\phi}$ is the flow profile and $\tilde{v}_{r,\theta} = v_{r,\theta} - \bar{v}_{r,\theta}$ is the fluctuating part of the radial (respectively poloidal) velocity, $\tilde{\psi}$ is the fluctuating part of the magnetic flux. The Reynolds stress $T_R = \langle \tilde{v}_\theta \tilde{v}_r \rangle_{\theta\phi}$ and the Maxwell tensor $T_M = \langle \partial_\theta \tilde{\psi} \partial_r \tilde{\psi} \rangle_{\theta\phi}$ are represented by the first two terms of Eq. (7). The r.h.s. of Eq. (7), T_V , corresponds to the viscosity effects while the last term corresponds to a friction with the imposed shear flow defined by v_{imp} . The latter is defined via its shear $\omega_{E \times B} = \omega_E \partial_x v_{imp} = \partial_r E_r / B_0 = \omega_E / \cosh(\sigma x)$ where $x = r - r_0$ and r_0 corresponding to the position where the shear is maximal. The shear amplitude is denoted by ω_E and the shear layer width σ is equal to 10% of the radial extension of the simulated zone. The velocity profile has been chosen such that it correspond to an experimental profile [13].

Fig. (5) shows the evolution of the confinement time (reflecting the dynamics of the pressure gradient), the normalized convective flux and the magnetic flux. Quasi-periodic relaxations are

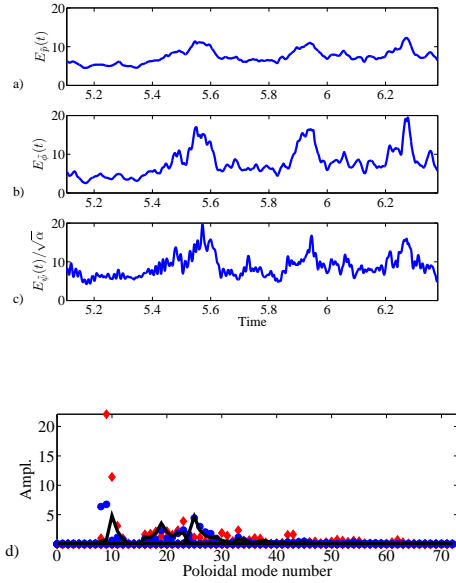


Figure 6: *Energy for pressure fluctuations (a), electrostatic (b) and electromagnetic potentials (c) vs time (in ms) for a typical run with relaxation oscillations. In this plot, the value of $\sqrt{\alpha}$ is 0.25. d) Spectra in function of the poloidal mode number before (solid line), during (diamond) and after (points) a relaxation event.*

observed and characterized by a growth of the confinement time on a long time scale and followed by a fast degradation. After these events, the transport barrier builds up again. During these losses of confinement, the time evolution of the convective flux Γ_{conv} and the magnetic flux $\Gamma_{\delta B}$ reveal the appearance of flux peaks corresponding to an increase of turbulent transport through the barrier. The relaxation frequency can be estimated, $f_{relax} \simeq 0.006\tau_{int}^{-1}$ corresponding to a frequency of the order of few kHz . This value is in agreement with experimental measurements of relaxation oscillations phenomena in tokamaks such as Type III ELMs, with frequencies ranging between 0.1 and 10 kHz [14]. The barrier relaxation have been found to be robust and appear in a wide range of parameter values [8]. The temporal dynamics of the energy associated with pressure fluctuations $E_{\bar{p}}$, the electrostatic potential fluctuations $E_{\bar{\phi}}$ as well as the electromagnetic perturbations $E_{\bar{\psi}}$ are plotted in Fig. (6a-c). This demonstrates that during the relaxation process, the magnetic activity is enhanced as it is the case in experimental observations of transport barrier relaxations [9, 10] where a simultaneous increase in magnetic fluctuations is associated to these relaxation events.

Fig. (6d) shows the power spectra of EM fluctuations for three phases : during the quiescent phase, during a relaxation and after this event. The growth of a mode at the barrier center is observed during a relaxation. This mode has a toroidal mode number $n = 4$ and a poloidal mode number $m = 10$ which correspond to a resonant mode on the surface defined by $q = m/n = 10/4$. Note that the mode which grows at the barrier center is the resonant mode with the lowest toroidal and poloidal mode numbers in the present simulations. The fact that, as in the ES case, a growth of a mode localized at the barrier center is observed suggests that the main mechanism behind this relaxation phenomena is similar in both cases: a perturbation at the barrier center exhibits a transitory growth due to a time delay in the shear flow stabilization [11, 12]. With the definition $\omega'_E = m(\xi_{bal}/r_0)\omega_E$, the characteristic growth time $\tau_D = (\chi_{\perp}\omega_E'^2/4)^{-1/3}$ is of the order of $10\tau_{int} \approx 0.02$ ms in our simulations which is of the same order of magnitude as the growth time of the flux peaks observed in Fig. (5b).

Over the last decade, the possibility of controlling ELMs has become plausible, as recent experiments were carried out on DIII-D, on JET and on TEXTOR [15, 16, 17]. These experimental studies obtained a qualitative control over the ELMs by imposing resonant magnetic perturbations (RMPs) at the plasma edge. However, in order to get any quantitative result, work has to be done in the understanding of the interplay between transport barrier relaxations and RMPs. In this part, we investigate numerically the effects of static resonant magnetic perturbations (RMPs) on transport barrier relaxation oscillations using an electrostatic version of the model (1,2), i.e. $\partial_t\psi = 0$ in (3). We use the geometry of the TEXTOR tokamak, and plasma parameters close to those used in typical experiments on this machine Note that the parallel

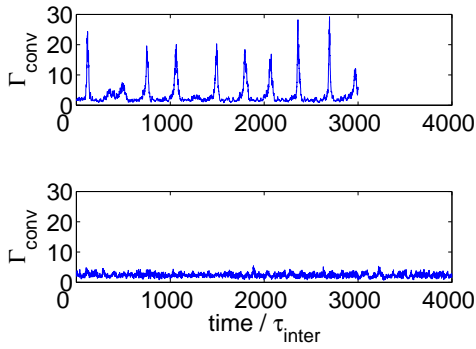


Figure 7: *Effects of RMPs on the dynamics of barrier relaxations: time traces of the radial heat flux in presence of an imposed mean shear flow with shear rate $\omega_E = 4$, without (a) RMP perturbation, with (b) $I_D = 1.5$ kA.*

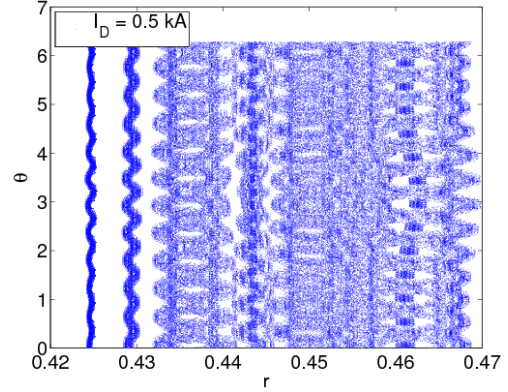


Figure 8: *Effects of RMP's on the topology of magnetic field lines : Poincaré map for a perturbation current $I_D = 0.5$ kA. Three residual magnetic island chains are observed, and a stochastic layer in between the central island chain and the one on the right.*

gradient in (1,2) is $\nabla_{\parallel} = \nabla_{\parallel 0} + \{\Psi_{RMP}, \cdot\}$, where $\nabla_{\parallel 0}$ is the component due to the unperturbed magnetic field, $\{\Psi_{RMP}, \cdot\} = \frac{\partial \Psi_{RMP}}{\partial x} \frac{\partial}{\partial \theta} - \frac{\partial \Psi_{RMP}}{\partial \theta} \frac{\partial}{\partial x}$ denote the Poisson brackets and the magnetic flux due to the resonant magnetic perturbation is written as: $\Psi_{RMP}(x, \theta, \varphi) \sim I_D \sum \Psi_m(x) \cos(m\theta - n_0\varphi)$ where $\Psi_m(x) = \frac{\sin(m-m_0)}{m-m_0} \exp(m_c x)$ is the spectrum of the RMPs, m_0 is the central poloidal harmonic number, m_c denotes the poloidal harmonic number of the RMP-producing coils, n_0 is the toroidal harmonic number. In the case studied here, we use $n_0 = 4$, with $q_{x=0} = q_0 = 3$, so that the central poloidal harmonic number is $m_0 = 12$. [18].

We propose the following model based on the balance of heat fluxes, to explain the behaviour of the convective flux and pressure gradient in the presence of RMPs and a shearflow-induced transport barrier. Taking into account RMPs, the pressure fluctuations should be further decomposed into an equilibrium and a turbulent part: $\tilde{p} = \tilde{p}^{eq}(x, \theta, \varphi) + \tilde{p}^{turb}(x, \theta, \varphi, t)$, and similarly for the radial velocity harmonics \tilde{v}_x . The energy balance (6) taken in a stationary state with $\Gamma_{\delta B}$ replaced by Γ_{RMP} can then be written:

$$\Gamma_{conv}^{eq} + \Gamma_{conv}^{turb} + \Gamma_{coll} + \Gamma_{RMP} = \Gamma_{tot} \quad (8)$$

where $\Gamma_{RMP} = \chi_{\parallel} \left\langle \frac{\partial \Psi_{RMP}}{\partial \theta} \nabla_{\parallel} p \right\rangle_{\theta, \varphi}$ represents the heat flux due to the magnetic flutter generated by the RMPs, $\Gamma_{conv}^{turb} = \langle \tilde{p}^{turb} \tilde{v}_x^{turb} \rangle_{\theta, \varphi}$, $\Gamma_{conv}^{eq} = \langle \tilde{p}^{eq} \tilde{v}_x^{eq} \rangle_{\theta, \varphi}$ are respectively the turbulent and equilibrium convective heat flux, where \tilde{v}_x denotes fluctuations of the radial velocity. Time series of the convective flux Γ_{conv} are presented, in presence of an imposed mean sheared flow, for different values of the divertor current I_D [Fig. 7]. In the reference case without RMPs, we observe heat bursts (Fig. 7b) which are associated with relaxation oscillations of the pressure profile and therefore also correspond to relaxations of the transport barrier. In the case with RMPs, we observe that the heat bursts are mitigated by the RMPs, (Fig; 7b). The amplitude of the heat bursts decreases and their frequency increases. It is found that the mitigation of the relaxation oscillations associated with the heat bursts is linked to a modification of the transport barrier geometrical properties. This modification is due mainly to a change of magnetic topology (Fig. 8), namely the presence of residual magnetic island chains and of a stochastic layer both induced by RMPs. An erosion of the pressure gradient profile is observed

at the surface of main resonance, e.g at the resonant surface $q = m_0/n_0$, where m_0 , n_0 are the principal poloidal wave-number and the toroidal wave-number of the RMPs, respectively. This erosion is shown to be linked to the presence of residual magnetic island chains inducing a stationary convective transport Γ_{conv}^{eq} of heat (and particles) in the radial direction. Far from the principal resonance surface but inside the shear-layer, the pressure gradient modifications depend if there is stochastic resonance overlap or not.

4. Conclusions.

In conclusion, turbulence simulations of a tokamak edge plasma have been realized focusing on the impact of electromagnetic fluctuations. The role of the α_N parameter has been analyzed by a study of the different stresses present in the equation for the poloidal plasma flow. A modification of the relative importance of Reynolds stress and Maxwell tensor depending on the value of α_N has been observed, leading to a decrease of the confinement time with increasing α_N . An increase of magnetic activity is observed during a relaxation event and the frequency range is of the same order as the one observed in the case of type III edge localized modes (ELMs) [14]. The physical mechanism underlying these relaxations remain the same as in the electrostatic case. Therefore, magnetic fluctuations have negligible influence on the relaxation process while the magnetic activity is enhanced by these relaxations. This reflects a complete scenario which agrees with experimental observations that show a clear evidence of the magnetic activity during the relaxations [5]. In the presence of RMPs, barrier relaxations are found to be stabilized. An erosion of the pressure gradient profile is observed at the surface of main resonance, e.g at the resonant surface $q = m_0/n_0$, where m_0 , n_0 are the principal poloidal wave-number and the toroidal wave-number of the RMPs, respectively. This erosion is shown to be linked to the presence of residual magnetic island chains inducing a stationary convective transport Γ_{conv}^{eq} of heat (and particles) in the radial direction. Far from the principal resonance surface but inside the shear-layer, the pressure gradient modifications depend if there is stochastic resonance overlap or not.

References

- [1] P. Beyer *et al.*, *Phys. Plasmas*, **8**, 4271 (1998).
- [2] J.W. Connor *et al.*, *Phys. Plasmas*, **5**, 2687 (1998).
- [3] U. Frisch, *Turbulence: The Legacy of A.N. Kolmogorov* (CUP, Cambridge, U.K., 1995).
- [4] R. Benzi, *et al.*, *Phys. Rev. E*, **48**, R29, (1993).
- [5] G. Y. Antar, *Phys. Rev. Lett.* **91**, 055002 (2003).
- [6] B. Labit *et al.*, *Phys. Rev. Lett.* **98**, 255002 (2007).
- [7] J. A. Krommes, *Phys. Plasmas* **15**, (2008).
- [8] G. Fuhr, PhD thesis, Univ. de Provence, 2006.
- [9] H. Zohm, *Plasma Phys. Control. Fusion*, **38**, 1213 (1996).
- [10] J.W. Connor *Plasma Phys. Control. Fusion*, **40**, 191 (1998).
- [11] P. Beyer *et al.*, *Phys. Rev. Lett.*, **94**, 105001 (2005).
- [12] P. Beyer *et al.*, *Plasma Phys. Control. Fusion*, **49**, 507 (2007).
- [13] Ch. P. Ritz, *Phys. Rev. Lett.*, **65**, 2543 (1990).
- [14] M. Becoulet *et al.*, *Plasma Phys. Control. Fusion*, **45**, A93 (2003).
- [15] T.E. Evans, R.A. Moyer, P.R. Thomas *et al.*, *Phys. Rev. Lett.* **92**, 235003 (2004).
- [16] Y. Liang, H.R. Koslowski, P.R. Thomas *et al.*, *Phys. Rev. Lett.* **98**, 265004 (2007).
- [17] K. H. Finken, B. Unterberg, Y. Xu *et al.*, *Nucl. Fusion* **47**, 522 (2007).
- [18] T. Habersheit, PhD Thesis, Univ of Bochum (2006).
- [19] R. Fitzpatrick, *Phys. Plasmas* **2**, 825-837 (1995).